Shock Compression of Plane Targets by Laser Ablation

C. G. M. van Kessel *

Max-Planck-Institut für Plasmaphysik, 8046 Garching bei München, Germany

(Z. Naturforsch. **30 a**, 1581–1593 [1975]; received October 14, 1975)

The properties of laser ablation driven shockwaves in plane transparent targets are investigated using high speed photography. The pressure, density and temperature of the compressed state behind the shockwave is determined with the shockwave Hugoniots of the target materials. The shockwave propagation is explained by a modified blastwave model and the energy transfer to the shock compressed region is estimated.

I. Introduction

Since the advent of the Q-switched laser in 1962 with the work of McClung and Hellwarth [1], the interaction of its powerful, focused output beam with solids has led to new concepts in the field of high-pressure, high-temperature physics. Well known is the use of laser radiation for the heating of small D – T pellets to achieve thermonuclear fusion conditions [2, 3]. The idea of compressing the pellet by convergent compression waves has particularly reduced the requirements on the laser energy to obtain a thermonuclear burn [4].

Other applications are the generation of shock waves of extreme pressures and temperatures in solids for investigating their equation of state under these conditions [5, 6], the simulation of meteorite impact on space vehicles [7] and high-pressure metallurgy [8].

Motivated in particular by the interest in laser-induced fusion, laser systems are now under construction which should deliver in the near future energies of 10^3 J in pulses of less than 10^{-9} s duration. Focussed onto the surface of a solid target, such powerful pulses should produce pressures of the order of 100 Mbar, this being well beyond the pressure range of standard techniques. An advantage of using lasers is the fact that high pressures can be achieved in light, compressible solids as well as in stiff materials. This is in contrast with the standard shock wave techniques, where the pressure is limited by the mismatch of the shock wave impedances of the driver medium and the target material. An additional advantage is the possibility of a programmed compression process by shaping the laser pulse with pulse stacking or other techniques [9]. For these reasons it is believed that lasers will soon become an alternative tool for generating extremely high pressures.

The phenomena which occur on irradiation of a solid target with a focused high-power laser beam have been described in many places (see the refs. of Section III a). Ionization and subsequent heating of a thin plasma layer lead, for the case of a single laser beam irradiating a plane target, to the typical flow pattern in Figure 1. Laser radiation penetrates

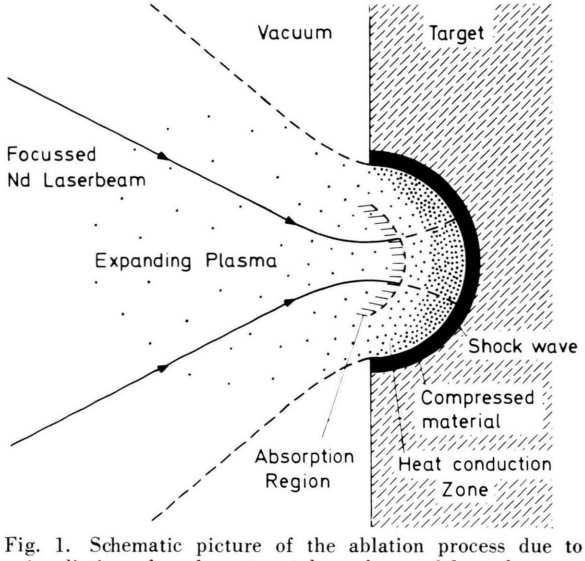

Fig. 1. Schematic picture of the ablation process due to irradiation of a plane target by a focussed laser beam.

through the expanding plasma to the absorption zone characterized by the socalled critical density (see Sect. II), where it is absorbed and partially reflected. Owing to the strong heating of matter in the absorption zone and owing to heating of even denser layers, which are not directly accessible to the laser radiation, by heat conduction (heat-conduction zone) a high pressure is exerted on the sur-

* Work supported by a Euratom grant. Reprint requests to Dr. R. Sigel, Max-Planck-Institut für Plasmaphysik, Experimentelle Plasmaphysik 4, *D-8046 Garching*, Germany.

rounding solid material. This leads to the formation of an intense shock wave which travels into the interior of the target. As a consequence of momentum conservation the momentum imparted to the compressed solid behind the shock front balances at each instant of time that of the outflowing plasma.

Initially, as long as the depth of the phenomenon is small compared to its lateral dimensions, the flow of matter will be plane.

When, with time, the characteristic length of the expanding plasma or the shock wave path exceeds the diameter of the absorption region, its initial plane geometry will be changed by lateral expansion waves and the complex structure of Fig. 1 is obtained. After termination of the laser irradiation the plasma will cool as a result of expansion and the ablation rate will decrease. The shock wave separates from the ablation surface and its intensity decreases owing to its spherical propagation to that of a weak shock wave which propagates with sound velocity.

During the past years most attention has been paid to the plasma or vapour in front of the solid where the energy is absorbed. However, as the compressed solid state is of main interest for the applications mentioned, additional knowledge is needed besides the existing results on the burn through time [10], crater size [11] or the observation of the plasma flow [12, 13], which gives only an indirect account of the behaviour of the compression wave.

In this paper we should like to discuss an experiment in which the laser driven shock wave in a plane target irradiated by a single beam was observed for the first time [14]. In Sect. II we describe the experimental results obtained by a high-speed photographic technique described earlier [15]. In Sect. III we describe the theoretical models used for evaluation of the shock wave parameters and their relation to plasma parameters measured previously in this experiment. In Sect, IV a detailed evaluation and interpretation of the experimental results is given. Section V summarizes the merits and shortcomings of the type of experiment described.

II. Experimental Results

a) Experimental conditions

The experiments were performed with the Garching multistage Nd-laser system which was used with an output energy of ≈ 12 J in a pulse with a half-width of 5 ns. Focused with an aspherical F/l lens the power density in the focal plane was 2×10^{14} W/cm^2. The diameter of the focal spot was measured in vacuum by a photographic technique to be $(40 \pm 10)\,\mu$m [16]. As plane, transparent targets, sticks with a (2×2) mm^2 square cross-section, made of poly methyl methacrylate $(C_3O_2H_8)_n$ (Plexiglass) and solid hydrogen (the latter extruded from a liquid helium cooled cryostat) were used. Unless otherwise stated the focal plane was close in front of the target surface at the position where the maximum back reflection of the laser light was observed [16].

b) Framing and streak photography of shock wave propagation

The laser ablation driven shock wave was observed with a streak and framing arrangement having the optical axis perpendicular to the main laser axis and consisting of a fast image converter streak camera and a dye laser for background illumination (Figure 2). The phenomena occurring inside the transparent target were recorded in streak pictures

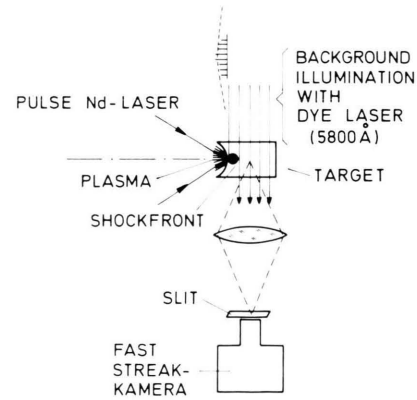

Fig. 2. The experimental arrangement.

with a narrow streak slit parallel to the main laser axis and the dye laser operating in the single pulse mode. Framing pictures were made with a wide-open streak slit and a pulsed background illumination obtained by mode-locking the dye laser. (As shown in Fig. 2, the target sticks had a slightly concave front surface to avoid distortions of the optical recording by the edges of the target sticks.) Further details of the laser system and the framing method may be found in [15] and [17].

Figures 3 and 4 * give examples of the streak pictures observed in both types of target material. The vacuum interface, the surface of the target on

* Figures 3, 4, and 7 on page Table 1582 a.

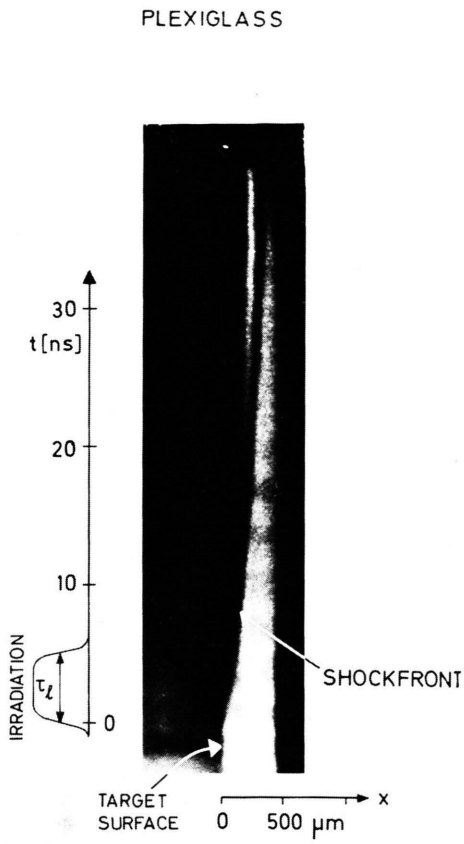

Fig. 3. Streak picture of an irradiated Plexiglass target. τ_l is the laser pulse duration.

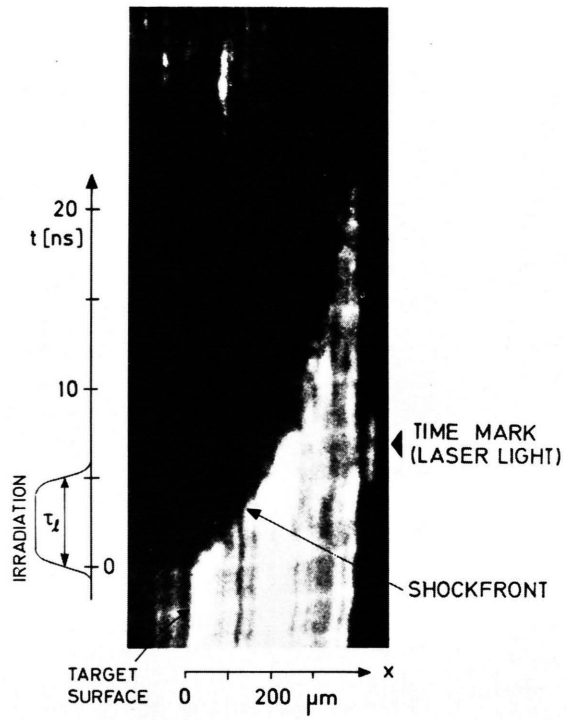

Fig. 4. Streak picture of an irradiated solid hydrogen target.

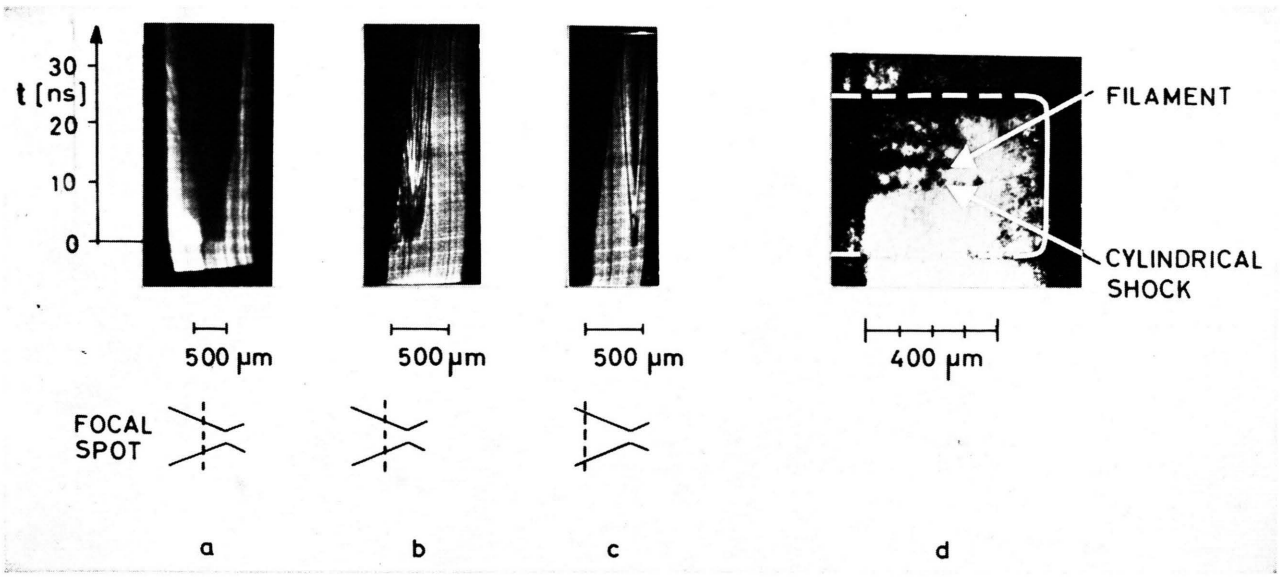

Fig. 7. Typical streak and framing pictures of an internal break down when the focussing position is inside the target. a) streak picture of a solid deuterium target, b) and c) streak pictures of a Plexiglass targed, and d) a single frame at ≈ 6 ns after onset of the irradiation of a Plexiglass target.

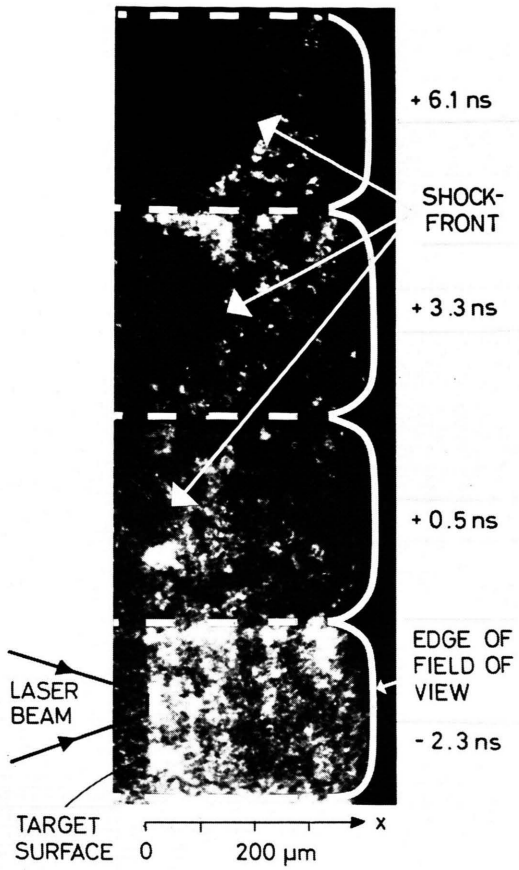

Fig. 5. Framing pictures of an irradiated solid hydrogen target.

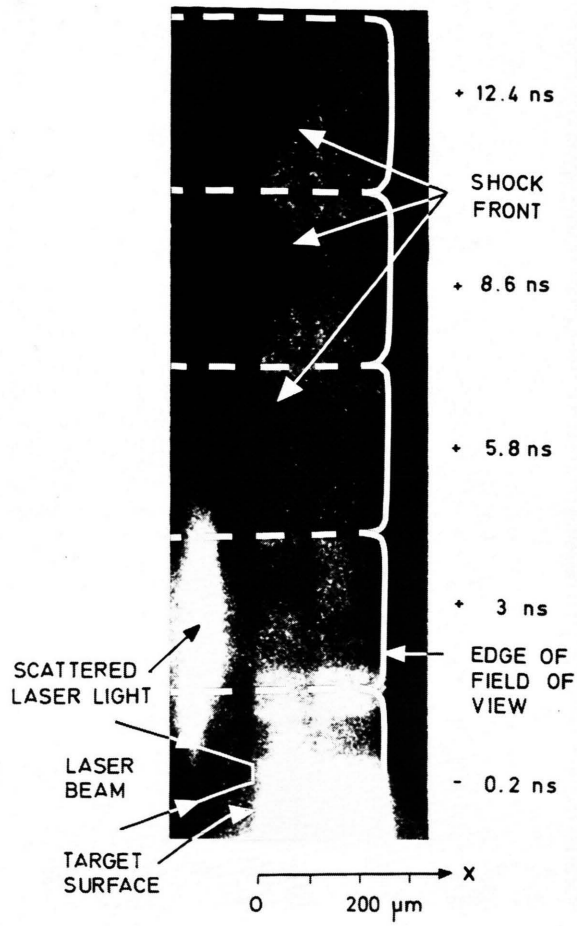

Fig. 6. Framing pictures of an irradiated Plexiglass target.

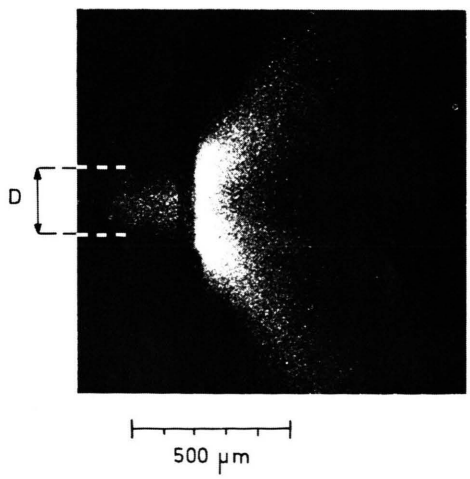

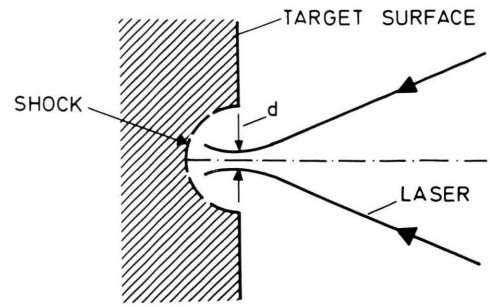

Fig. 15. Photograph of the X-rayemission of the plasma by a pinhole camera [37]. In the schematic picture the shock front position at the end of the irradiation is given. The diameter of the focal spot —d— and of the core plasma —D— are indicated.

which the laser beam is focused, remains undisturbed up to the time $t=0$, when the irradiation with the Nd laser begins. Simultaneously with the irradiation a shadow propagates into the interior of the target. The leading edge of this shadow is identified as the shock front (see the discussion in Section IVa). The duration of the laser irradiation is indicated on the left-hand side of the streak pictures. (The accuracy of the time correlation, provided either by stray laser light or by guiding light with a light pipe to the edge of the streak slit, is ± 1 ns.)

The velocity of the shock wave has the highest value at the start of irradiation and shows a steady decrease afterwards. The shock velocity in solid hydrogen is higher owing to the low initial density of the material. For the given examples the shock wave has already propagated more than 100 μm in Plexiglass and 200 μm in solid hydrogen when the laser radiation is terminated.

In the streak picture of an irradiated Plexiglass target a double structure with a transparent layer in between is observed after 20 ns. As we shall see (Sect. IVa), the shock wave is separated from the crater at these times.

The framing pictures in Fig. 5 and 6 ** give in a sequence of single pictures with a time interval of 2.8 ns the two-dimensional structure of the expansion of the shock wave during irradiation by the Nd laser. The focusing cone with the focal spot on the vacuum target interface is indicated. On the right-hand side of the picture the time of exposure for every frame relative to the start of irradiation is given. When the initially plane shock wave has travelled more than the diameter of the absorption zone it will assume a curved, approximately hemispherical shape. This is already observed during the laser pulse for the shock wave in hydrogen. In the last two frames of the picture shown the radii are 150 and 215 μm at 3.3 and 6.1 ns, just before and after the termination of the laser pulse.

c) *Internal breakdown and self focusing*

Shock waves with a regular structure such as that observed in Fig. 3 and 4 were observed with the focal plane at or in front of the target. It was noticed that the maximum shock velocity at the start of irradiation had its highest value with the position of the focal plane at that position which also yielded a maximum in back-reflection of the laser light [16].

When the focal spot was a certain distance inside the target internal breakdown and self-focusing phenomena were observed. Some examples are given in Fig. 7 a – d. In Fig. 7 a and 7 b the focal spot is only 300 and 200 μm respectively beyond the target surface and breakdown inside the solid occurs before the laser light is absorbed in the plasma created at the surface. When the focus was further inside the target a string of breakdowns along the laser axis, probably due to self-focusing, was recorded [18]. The single frame at about 6 ns after the onset of irradiation in Fig. 7 d shows a self-focusing filament surrounded by a cylindrical shock wave as the envelope of the spherical waves launched from each breakdown.

III. Theoretical Description of Laser-Target Interaction

a) *General considerations*

The gasdynamic flow induced by laser heating of a solid target has been investigated theoretically by analytical [19, 20] and numerical [17, 21] methods. According to these investigations the typical density and temperature profiles shown in Fig. 8 are found.

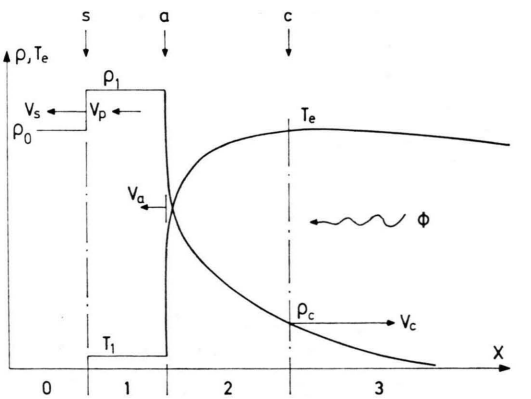

Fig. 8. Schematic density ϱ and electron temperature T_e profiles of the laser ablation process. The incident laser light Φ is incident from the right.

We distinguish four regions according to different states of matter:

- the undisturbed solid (0) bounded by the shock front (s),
- the shock compressed region (1) bounded by the ablation surface (a),
- the overdense heat conduction zone (2) bounded by the critical density (c) layer and
- the underdense expanding plasma (3).

This picture reproduces the flow along the main laser axis in Figure 1.

** Figures 5, 6 and 15 on page Table 1582 b.

Laser radiation with an optical frequency ω_l can penetrate a plasma only up to the layer with the electron density n_c where the incident light will be strongly damped by reflection and absorption over a distance of the order of a wavelength. At this electron density $n_e = n_c$, the critical density, the corresponding electron plasma frequency ω_p given by

$$\omega_p = \left((4\pi n_e e^2)/m_e\right)^{1/2}$$

is equal to the laser frequency ω_l (e is the elementary charge and m_e the electron mass). For a Nd laser with $\lambda = 1.06\ \mu$m, one obtains $n_c = 10^{21}\ \mathrm{cm}^{-3}$.

Though laser light absorption in the underdense plasma is not completely understood at present, it is generally believed that the main energy deposition occurs in the near vicinity of the critical layer, where absorption due to inverse bremsstrahlung [22], resonant absorption [23] and parametric instabilities [24] may take place. The electron temperature is thus expected to have a maximum in this layer.

From this absorption region heat diffuses either into the overdense or underdense plasma by nonlinear heat conduction. In this way the heat conduction connects the absorption region with the shock compressed region by the formation of the overdense plasma. (Note the large difference between solid and critical density.) As has been shown in [21], nearly all of the deposited energy diffuses first into the overdense plasma, where it leads to ablation of the compressed material, and then reappears as convective flow through the critical layer. The thermal pressure drives, together with the momentum of the ablated material, the shock wave which travels in the opposite direction to the ablated and expanding plasma and compresses the undisturbed solid material.

For a given laser intensity and wavelength exact profiles of the flow parameters can be calculated from the gasdynamic equations if laser light absorption and heat conduction are included. This has been done in [21] but only for the cases of plane and spherical flows. Thus, the applicability of the existing theoretical solutions to the experimental case where the plasma flow with time becomes two-dimensional (as illustrated by Fig. 1) is limited. In the present situation, i. e. with a lack of directly applicable two-dimensional computer solutions it is nevertheless possible [1] to evaluate the shock wave parameters from the experimental observations [2], to show how their maximum values can be connected with the plasma parameters near the critical density [3], to describe the shock wave decay after termination of the laser pulse by analytical solutions originally developed for the case of micrometeorite impact and, finally (in Sect. IV) [4], to show that in this manner a very reasonable understanding of the experimental observations is obtained if allowance for two-dimensional effects during irradiation is made.

b) The compressed solid behind the shock front

Along the shock the Hugoniot relations can be applied to determine the state of the compressed solid behind the shock front. For a small planar element of the shock moving with the velocity v_s into the undisturbed solid these relations are (Fig. 8)

$$\varrho_0 v_s = \varrho_1 (v_s - v_p), \tag{1}$$

$$\varrho_0 v_s^2 = \varrho_1 (v_s - v_p)^2 + p_1, \tag{2}$$

$$\varepsilon_1(\varrho_1, p_1) - \varepsilon_0(\varrho_0, p_0) = \tfrac{1}{2} p_1 \left(\frac{1}{\varrho_0} - \frac{1}{\varrho_1}\right) \tag{3}$$

with v_p the particle velocity, ϱ the density, p the pressure and ε the specific internal energy with subscripts 0 and 1 for the region ahead and behind the shock front respectively [25]. The initial pressure of the undisturbed solid may be neglected since $p_1 \gg p_0$.

From these relations the state behind the shock front can be determined from the shock velocity and the initial density if Eq. (3) is explicitly known in the form of the Hugoniot curve presenting the shock pressure as a function of the compression ratio for the initial density and pressure used. For a certain number of solids the Hugoniot curve has been determined from experiments in which, beside the shock velocity, a second parameter of the shocked state was measured. For Plexiglass this has been done up to shock pressures of 1.2 Mbar [26]. Since the pressure in our case is slightly higher, the Hugoniot curve for this material was extrapolated with the empirical relation between shock velocity and particle velocity

$$v_s = a + b\, v_p$$

which showed a good fitting to the existing curve with $a = 3.07 \times 10^5$ cm/s and $b = 1.295$.

For hydrogen the Hugoniot curve has only been measured up to 40 kbar [27]. To obtain the required curve, we have to resort to a theoretical equation of

state as calculated by Kerley for deuterium over a wide range of densities and temperatures [28]. For every couple of this theoretical isotherms $\varepsilon = \varepsilon(T_i, \varrho/\varrho_0)$ and $p = p(T_i, \varrho/\varrho_0)$ with temperatures T_i ranging from $1.78 \times 10^2 - 10^6$ °K a point on the Hugoniot curve is determined by calculating the value of the function

$$f(T_i, \varrho/\varrho_0) = \varepsilon - \varepsilon_0 - \tfrac{1}{2}(p + p_0)\,(1/\varrho_0 - 1/\varrho)$$

for different values of the compression ratio ϱ/ϱ_0. The values of ϱ and p for which $f(T_i, \varrho/\varrho_0)$ is identical to zero is by definition a point on the Hugoniot curve. On the assumption that hydrogen and deuterium have a similar behaviour for shock compression, the curve has been scaled with the initial densities and the known weak shock wave data [27]. The resulting Hugoniot curve for hydrogen is shown in Fig. 9 together with the curve used for

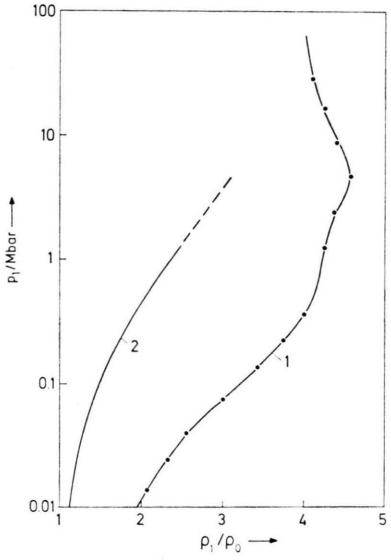

Fig. 9. Hugoniot curves for solid hydrogen (1) ($T_0 = 4$ K and $\varrho = 0.089$ g cm^{-3}) and for Plexiglass (2) ($\varrho = 1.18$ g cm^{-3}).

Plexiglass. The high compressibility of hydrogen causes such shock wave heating that at about 170 kbar dissociation, and at about 700 kbar ionization, changes the state behind the shock wave. As a result, the Hugoniot curve passes with increasing pressure a maximum in compression of 4.6 at 5 Mbar [25].

The Hugoniot curve can now be used together with the equation

$$p_1 = \varrho_0 v_s^2 (1 - \varrho_0/\varrho_1), \qquad (4)$$

which is obtained from Eqs. (1) and (2), to yield the relations $p_1 = p_1(v_s, \varrho_0)$ and $\varrho_1 = \varrho_1(v_s, \varrho_0)$ for determinating the state behind the shock wave as a function of the measured shock wave velocity.

It should be noted that although the determination of compression ratio for solid hydrogen might involve a certain unaccuracy due to using the whole procedure for getting the Hugoniot curve, the pressure determination is quite accurate owing to its weak dependence on the density ϱ_1 at high compression ratios [see Equation (4)]. To determine the temperature behind the shock wave, a plot of the experimental data for Plexiglass from [29] has been used, whereas the temperature of the shock compressed hydrogen was part of the Hugoniot curve calculation.

c) Relations between the parameters of the shocked state and the critical layer

In this section we are interested to find a relation which connects the electron temperature at the critical layer, which has already been measured [30], with the pressure behind the shock front. For this purpose we consider the heat conduction zone (2) in Figure 8.

For a step-like rising laser pulse the plasma flow is initially strongly non-stationary owing to a heat wave penetrating into the solid followed by the expansion wave. The characteristic time τ_H after which the expansion wave overtakes the heat wave and establishes a quasi-stationary flow in the heat conduction zone can be estimated according to [31]

$$\tau_H \cong 3 \times 10^{-32}\, \Phi$$

where the laser light flux Φ is in erg cm^{-2} s^{-1}. For $\Phi \cong 10^{21}$ erg cm^{-2} s^{-1} we find $\tau_H = 3 \times 10^{-11}$ s, i.e. τ_H is much smaller than the laser pulse duration and even the pulse rise time. Furthermore, as has been discussed in [20], the characteristic time τ_{pe} for establishment of a quasi-stationary flow of the expanding plasma can be estimated by $\tau_{pe} \cong R/C_{pe}$, where R and C_{pe} are the lateral extension and sound velocity of the expanding plasma. With typical values $R \cong 10^{-2}$ cm and $C_{pe} = 2 \times 10^7$ cm s^{-1} we find $\tau_{pe} \cong 0.5$ ns, a time comparable with the pulse rise time, but still small compared with the laser pulse duration. Thus, if we assume a quasi-stationary and plane flow through the heat conduction zone (the latter assumption being much less stringent than the assumption of a plane flow throughout the

expanding plasma), we can apply the mass and momentum conservation relations

$$\varrho_1(v_a - v_p) = \varrho_c(v_c + v_a), \tag{5}$$

$$p_1 + \varrho_1(v_a - v_p)^2 = p_c + \varrho_c(v_c + v_a)^2, \tag{6}$$

for the overdense region between the shocked state and the critical density. As indicated in Fig. 8, v_a is the propagation velocity of the ablation surface, p_c and ϱ_c are the pressure and the density in the critical layer and v_c is the expansion velocity in this layer.

From these relations and Eqs. (1) and (2) it is readily found that for $\varrho_1 > \varrho_0 \gg \varrho_c$

$$(v_a - v_p)/v_p < \sqrt{\varrho_c/\varrho_1} \ll 1$$

thus showing that the ablation surface moves nearly with the particle velocity inwards. In other words the ablation surface may be considered as a weakly leaking contact surface and the second term on the l.h.s. of Eq. (6) may be neglected when compared with the pressure p_1. Similarly, it can be shown that

$$|v_c + v_a| / v_a \gtrsim \sqrt{\varrho_0/\varrho_c}$$

thus showing that the motion of the ablation surface is small when compared with the escape velocity of the low density plasma at the critical density.

On the assumptions made above, we finally obtain from (6)

$$p_1 = p_c(1 + M^2) = n_c k T_e (1 + M^2)$$

where $M = v_c/c_T$ is the Mach number at the critical density layer. The contribution of the ions to the pressure has been neglected, as suggested by numerical simulations [21]. It may be noted that the right hand side of Eq. (7) no longer contains parameters of the shock wave region, which means that the approximations made above correspond to a situation where the ablation occurs from an incompressible (or infinitely dense) solid. In Sect. IVc formula (7) will be used to compare the measured electron temperature at the critical layer with the pressure behind the shock front and to calculate the Mach number.

The results of a computer simulation [21] in plane geometry are given in Fig. 10 in terms of p_1 and the maximum electron temperature near the critical layer. The shaded region contains results of the simulation at different times (0.5 – 4 ns after the onset of laser irradiation), the corresponding laser intensities being indicated as well. This figure will

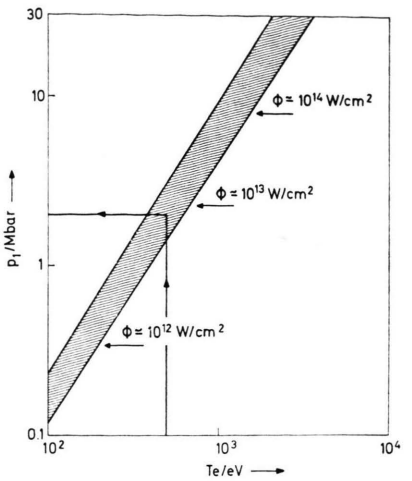

Fig. 10. One-dimensional plane computer simulation results presenting the shock pressure p_1 as function of the electron temperature T_e at the critical layer. The laser intensities Φ used in the different simulations are given (Courtesy Dr. P. Mulser).

enable us later (Sect. IVc) to relate the measured pressures and temperatures to the laser intensity incident on the plasma. It should be noted that the relation (7) is well confirmed by the simulations.

The fractional energy transfer is defined by the time rate of work on the solid divided by the time rate of absorbed energy I:

$$\eta_{ab} = \frac{p_1 v_p}{I} \frac{p_1^{3/2} \sqrt{(1 - 1/\varkappa)/\varrho_0}}{I} \tag{8}$$

where Eqs. (1) and (2) have been used to eliminate v_p. $\varkappa$ is the compression ratio ϱ_1/ϱ_0.

The time rate of absorbed energy appears approximately as the flux of the total enthalpy of the flow at the critical layer. This follows from the considerations that under the condition of a quasi-stationary hydrodynamic flow the energy contents of the overdense region changes only slowly and, as has been shown in [21], the losses due to heat conduction directly towards the low density expanding plasma do not exceed 10%. Additionally, only a small part of the incident laser energy is transferred to the compressed solid ($\eta_{ab} \ll 1$ as will be found). With an equal ion and electron temperature we therefore obtain

$$I = \varrho_c v_c(\varepsilon_c + p_c/\varrho_c + \tfrac{1}{2} v_c^2) = M(4 + \tfrac{1}{2} M^2)\varrho_c c_T^3.$$

With Eq. (7) the efficiency of the ablation process can thus be expressed as

$$\eta_{ab} = \sqrt{1 - 1/\varkappa} \frac{(1 + M^2)^{3/2}}{M(4 + \tfrac{1}{2} M^2)} \sqrt{\frac{\varrho_c}{\varrho_0}} \tag{9}$$

or with $\varkappa \cong 4$ and $M \cong 1$

$$\eta_{ab} \cong \tfrac{1}{2} \sqrt{\varrho_c/\varrho_0}\,.$$

Inserting $\varrho_0 \approx 50\,\varrho_c$ we see that the ablation efficiency is about 7%, which indicates that only a small part of the absorbed energy is transferred to the compressed solid state.

d) Late stage decay of the shock wave

The late stage of shock wave propagation may be expect to have a similarity to the propagation of a shock wave due to a point-explosion at the target surface because the diameter of the absorption region and the laser pulse duration have lost their meaning as characteristic quantities of the process.

Well known are the blast wave solutions by Sedov [32] and Taylor [33] for perfect gases based on the self-similarity principle. In their approach the functional dependence of the shock wave path R_s follows from dimensional considerations and is given by

$$R_s(t) = \left(\frac{25\,\alpha(\gamma)\,E_0\,t^2}{8\,\pi\,\varrho_0} \right)^{\frac{1}{5}} \qquad (10)$$

where ϱ_0 is the initial gas density. The dimensionless coefficient $\alpha(\gamma)$ can be obtained from the fact that the total energy E_0 involved is conserved during the process. The value of $\alpha(\gamma)$ has been tabulated for values of the specific heat ratio γ ranging from $2-100$ in [34].

A basic assumption for the application of the self-similarity principle is constancy of the compression ratio ϱ_1/ϱ_0 across the shock front, which is certainly valid for strong shock waves in perfect gases [and amounts to the value $(\gamma+1)/(\gamma-1)$]. But as can already be seen from the Hugoniot curves presented before, for solids this will only be the case at extremely high shock pressures.

The blast wave solution has been modified by Rae and Kirchner [34, 35] in order to apply it to a solid, the shock wave properties of which can be described by the simple empirical relation

$$v_s = a + b\,v_p\,. \qquad (11)$$

A large number of solids, including Plexiglass, are well approximated by this relation, which may stand for the third Hugoniot relation (3).

In the modified solution the change of the density behind the shock is taken into account by varying the value of γ in the expression of the self-similar solution (10) as the shock wave propagates. By means of the relation (11) γ and, hence the density ϱ_1, becomes a function of the shock velocity:

$$\gamma = \frac{\varrho_1+\varrho_0}{\varrho_1-\varrho_0} = 2\,\frac{v_s}{v_p} - 1 = \gamma\left(\frac{v_s}{a}, b\right).$$

When this is introduced in the equation for $\alpha(\gamma)$, the solution will be consistent at the shock front with the Hugoniot relations in terms of shock wave compression and pressure. This modification can be understood as an attempt to match instantaneously the real solution with a series of similarity solutions at each time corresponding to a perfect gas with an apparent value for γ, but each corresponding to the same total energy E_0.

The final solution has been tabulated in dimensionless form for several values of the parameter b in [34].

Originally, this modified blast wave approach was developed to describe the late-stage shock wave propagation of the hypervelocity impact process but, as will be shown in Sect. IVd, the procedure can also be successfully applied to the case of shock waves induced by pulsed laser irradiation in stiff target materials like Plexiglass.

IV. Evaluation and Interpretation of the Experimental Results

a) The opacity behind the shock front

Before we procede with the evaluation of the experimental results, the opacity of the region encompassed by the shock wave will be discussed in order to explain the shadows observed in the streak and framing pictures. For this purpose we consider the transparency of the structure, as depicted in Fig. 1, to the parallel beam of the background illumination. As long as the electron density in the core plasma exceeds $3\times10^{21}\,\mathrm{cm}^{-3}$ (the critical density for $\lambda = 580\,\mathrm{nm}$ of the dye laser), the illumination light cannot penetrate the plasma more than a single wavelength and the plasma core will be completely opaque.

Concerning the transparency of the shock-compressed region, at high shock intensities, shock heating may cause thermal dissociation and ionization, whereas shock compression may cause a closing of the energy gap between conduction and valence band leading to the "metallization" of an insulator owing to the reduced interatomic spacing. For Plexiglass a sharp increase of its electrical conduc-

tivity by 20 orders of magnitude has been observed for shock wave intensities of more than 800 kbar, which was partly due to the onset of "metallization" [36]. The high compressibility of solid hydrogen leads to a strong shock wave heating causing thermal dissociation and ionization of the compressed material. As may be calculated from the equation of state given by Kerley [28], the electron density will exceed $10^{22}\,\mathrm{cm}^{-3}$ for shock waves stronger than 700 kbar. Therefore, we arrive at the result that for both types of target material the shock-compressed region will also be opaque for shock intensities exceeding the stated values, and that only an overall shadow will be observed.

These considerations and the good agreement of the measured shock wave parameters, evaluated below, with the plasma models confirm the assumption that the leading edge of the observed shadow may be identified as the shock front.

After the laser pulse the ablation process will come to an end and the shock wave will propagate with decreasing intensity. Below a certain shock intensity the shock-compressed region will become transparent but at this stage lens effects have to be taken into account because of the curvature of the shock front. A simplified model for the refraction of background light is the refraction of a parallel beam on a homogeneous sphere in a medium of lower density with refraction indices n' and n, respectively, corresponding to the densities behind and ahead of the shock front. The incident parallel light rays are subjected to refraction over a total angle Θ according to

$$\Theta = 2\left(\arcsin\frac{r}{R_s} - \arcsin\frac{r\ n}{R_s\ n'}\right)$$

where R_s is the shock front radius, and r the off-axis distance of the incident light ray. Light rays at grazing incidence (i. e. for $r = R_s$) will have the maximum refraction angle Θ_{max} and if this angle is larger than the viewing angle of the optical recording system, the light ray with $r = R$ will not reach the film plane. Therefore, given the compression ratio and the viewing angle, a certain thickness of shock-compressed region is required to allow a light ray through this region to be recorded.

This explains the double structure observed at the late stage in the given streak picture example of an irradiated Plexiglass target. The shock wave separated from the plasma-filled crater has a thin opaque zone behind it owing to lens effects and is not to be connected with the thickness of the shock front itself, which is expected to be small compared with the wavelength of visible light [29].

b) Evaluation of density, pressure and temperature history behind the shock front

The position of the shock front was determined from enlarged streak pictures and the shock wave velocity as a function of time by means of a goniometer. Figures 11 and 12 give the results for the

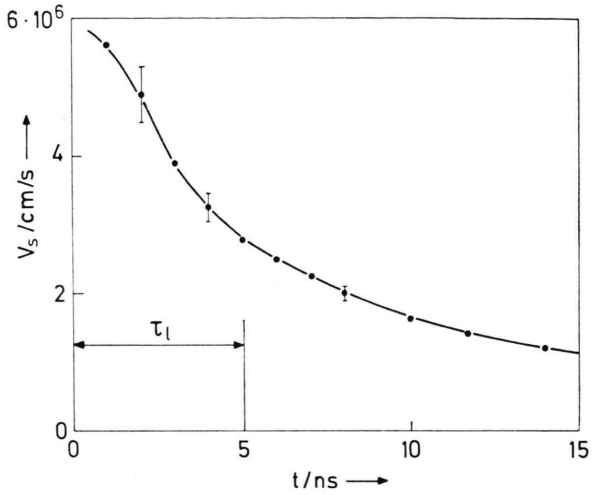

Fig. 11. The measured shock velocity v_s as function of time for a solid hydrogen target. The laser pulse duration is indicated by τ_l.

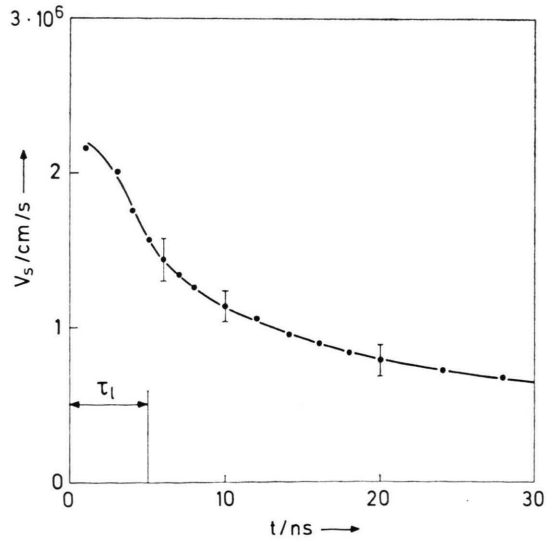

Fig. 12. The measured shock velocity v_s as function of time for a Plexiglass target. The laser pulse duration is indicated by τ_l.

shock wave velocity averaged over four identical shots with a laser energy of 12 ± 2 J. The scattering of the data, mainly due to the non-reproducibility of the laser energy, has been indicated for several times. The velocity has a maximum value at the start when the onset of motion is observed and decreases afterwards. The maximum shock velocities are 5.8×10^6 cm/s in solid hydrogen, and 2.3×10^6 cm/s in Plexiglass. With the Hugoniot curves given in Sect. III b the shock velocity results can be translated into the pressure, density and temperature behind the shock front as a function of time. The results are shown in Figs. 13 and 14. For a solid hydrogen target a maximum pressure of 2Mbar and a compression rate of 4.3 are obtained. In Plexiglass the maximum pressure achieved is 4 Mbar for a compression of 3.0. The obtained values are slightly higher than in [14] because a revised Hugoniot curve from additional shock data was used.

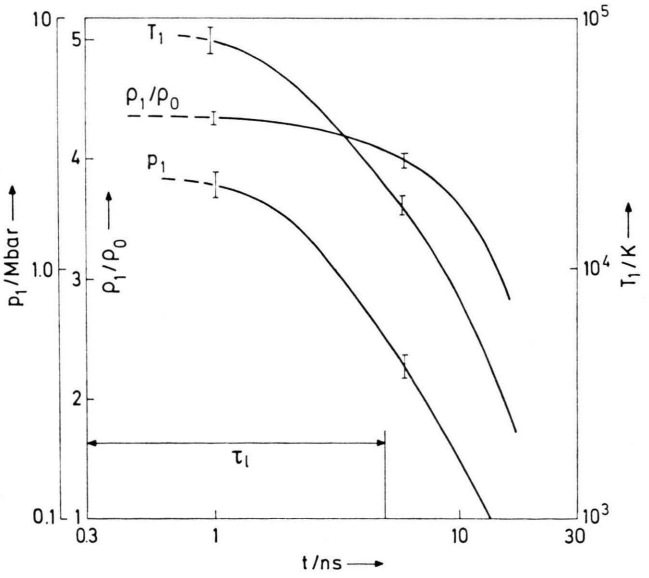

Fig. 13. The pressure p_1, the compression ratio ϱ_1/ϱ_0, and the temperature T_1 behind the shock front as function of time for a solid hydrogen target (τ_l is the laser pulse duration).

c) The overdense heat conduction region

Under the assumption of a plane and quasi-stationary flow in the overdense heat conduction region we relate the evaluated maximum pressure at the initial stage of irradiation to the previously measured temperatures [30, 37]. With an experimental electron temperature of 500 eV * the pressure at the critical layer is given by $p_c = n_c k T_e = 800$ kbar.

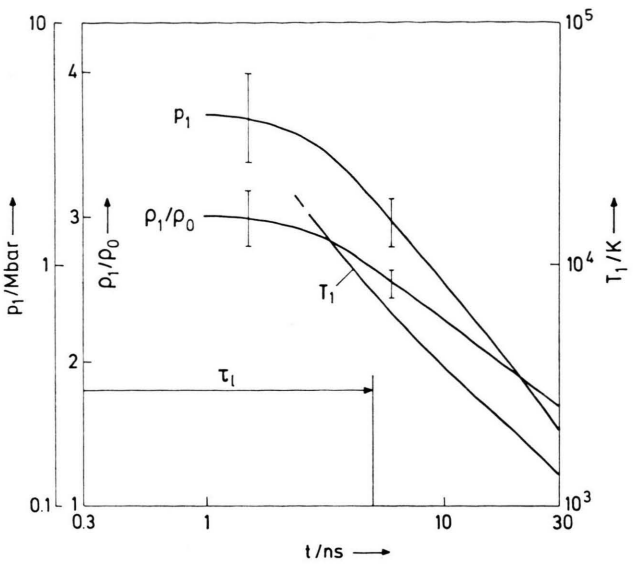

Fig. 14. The pressure p_1, the compression ratio ϱ_1/ϱ_0, and the temperature T_1 behind the shock front as a function of time for a Plexiglass target (τ_l is the laser pulse duration).

Relating this value to the maximum pressure behind the shock front of Sect. IVb using the formula (7), we obtain for the Mach number for solid hydrogen $M = 1.2 (\pm 0.5)$ and for Plexiglass $M = 2.0 (\pm 0.5)$. The uncertainty is due to the limited accuracy in the determination of the shock velocity and the electron temperature, the latter, from X-ray measurements, being complicated by the presence of a non-Maxwellian tail in the electron distribution of the plasma. From the Mach numbers it is seen that the recoil of the flow in the overdense region appreciably enhances the pressure in the shock-compressed region.

With the electron temperature as a basis for comparison, the computer simulation results presented in Fig. 10 predict reasonably well the pressure behind the shock wave and also the Mach number evaluated above. It is noteworthy, according to the computer simulation, a laser intensity of about 10^{13} W/cm^2 only is necessary to produce the measured data.

The discrepancy between this value and the vacuum laser intensity of 2×10^{14} W/cm^2 used in the experiment may be understood with the help of recent time-integrated X-ray pinhole photographs of

* The measurements of [30] were performed at a higher laser intensity. The value used was obtained by the experimental law $T_e \sim \Phi^{0.33}$.

the plasma [37, 38]. Figure 15 shows an example of the recorded soft X-ray emission pattern from an irradiated solid deuterium target. For comparison, the shock front position just after the laser pulse, obtained from a framing picture and scaled for solid deuterium, is given in the picture. The X-ray pinhole photographs, which are evaluated in detail in [37], show that the plasma structure consists of a conical outflow and a plasma-filled crater. The diameter of the core plasma is five times as large as the diameter of the focal spot in vacuum (see Figure 15). This indicates that plasma heating and ablation occur on a much larger area than the minimum focal spot area. This effect which we attribute to lateral heat conduction, results in an effective flux density much lower than the vacuum laser flux density. In addition, the lateral spread of the outflow reduces the thrust of the expanding plasma normal to the target.

It is concluded from these results that the temperatures and pressures achievable in plane target experiments with sharply focused, intense beams are overestimated by idealized, plane computer simulations unless a reduction of the effective laser intensity (compared with its maximum vacuum value) due to the two-dimensional nature of plasma flow is taken into account. This is supported by the results presented in [39], where agreement of experimental and computational results could be obtained only for laser flux densities $1-2$ orders of magnitude lower than the maximum vacuum laser flux density. It should be noted that we attribute the reduction of the effective flux density to hydrodynamic effects, in particular lateral heat conduction, rather than to laser light refraction in the plasma since recent, spatially resolved photographs of second harmonic emission of the main laser light have shown that the area of the critical layer exposed to laser irradiation may be as small as the vacuum focal spot diameter [40].

Finally, it should be mentioned that the experimental results allow us, at best to a certain extent, to check the validity of the assumptions made above, in particular the assumption of a plane flow in the overdense region. As can be verified from the framing pictures of Plexiglass, at the time of maximum pressure the distance covered by the shock wave is small compared with its lateral extent. In addition, it has been observed in interferometry [41] and Schlieren [42] experiments that the critical density layer stays inside the crater or just in front of the target surface (at a distance $<20\,\mu$m). Therefore, in the case of Plexiglass the assumption of a plane flow in the overdense region seems to be well justified during the first part of the laser pulse. In the case of solid hydrogen this assumption is more difficult to assess, because the shock front rapidly assumes a hemispherical shape and the relative distance of the shock front and critical layer inside the crater is not known at present.

d) The efficiency of energy transfer to the shock-compressed region

In solid hydrogen the shock wave propagates, as has been observed in the framing picture in Fig. 5, with an approximately hemispherical wave front with its centre in the vicinity of the target surface. Given this simple geometry, it is easy to estimate the kinetic energy KE transferred to the shock compressed region.

As discussed in Sect. III c, the density decreases rapidly behind the ablation surface and only a small portion (about 4%) of the involved material flows out into the vacuum as hot plasma. Therefore, almost the entire mass encompassed by the shock wave is concentrated in a thin layer behind the shock front. On the assumption that the density inside this layer is constant and equal to the density behind the shock front, the thickness of the layer Δr is given by the conservation of mass

$$\tfrac{2}{3}\pi R_s^3 \varrho_0 = 2\pi R_s^2 \Delta r \varrho_1 , \quad \text{or} \quad \Delta r = \frac{R_s}{3}\frac{\varrho_0}{\varrho_1} .$$

Since for $\varrho_1 \gg \varrho_0$ we have $\Delta r \ll R_s$ we can consider this layer as being thin (at least during the laser pulse) and its mass as moving with the particle velocity behind the shock front. Its kinetic energy is then equal to

$$\mathrm{KE} = \tfrac{1}{2} M v_p^2 \cong \tfrac{1}{3}\varrho_0 \pi R_s^3 \left(\frac{\varrho_1 - \varrho_0}{\varrho_1}\right)^2 v_s^2 .$$

Using the values for R_s, ϱ_1 and v_s already obtained from the measurements, the kinetic energy was calculated and the resulting curve is given in Figure 16. Near to the end of the laser pulse it shows a maximum of .5 J.

An equal amount of energy is also imparted as internal energy to the flow behind the shock front, as can be seen by neglecting the initial pressure p_0 in the Hugoniot relations (1), (2), and (3). The total energy transferred then has a maximum of 1 J, which is 8% of the total incident laser energy.

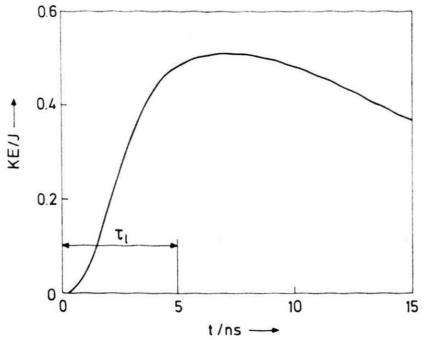

Fig. 16. The kinetic energy KE of the shock compressed region for a solid hydrogen target as function of time.

With the modified blast wave approximation developed by Rae and Kirchner and described briefly before, shock wave trajectories were calculated for the case of Plexiglass for several values of the total energy E_0 involved. In applying their solution the parameters $a = 3.07 \times 10^5$ cm/s and $b = 1.2$ were used. It was found (see Fig. 17) that the value of

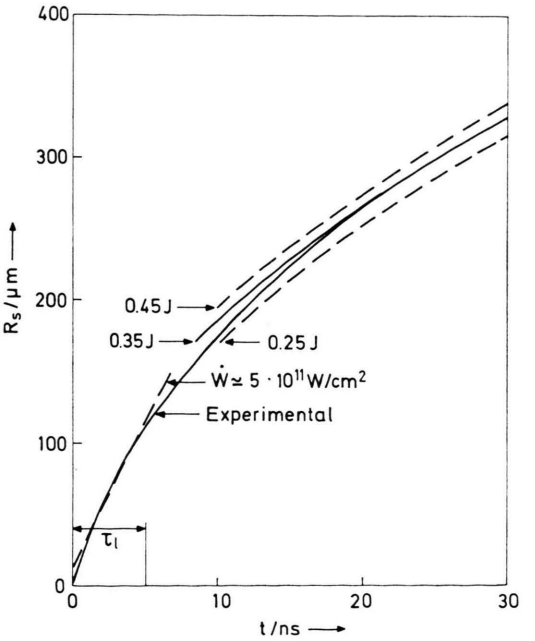

Fig. 17. The experimental shock wave trajectory in a Plexiglass target compared with the blast wave approximation at the late stage for $E_0 = .35 \pm .1$ J.

$E_0 = .35$ J furnished an excellent description of the late-stage propagation of the shock wave. For comparison the shock wave trajectories for $E_0 = .25$ and .45 J are also given as dashed curves. In this case of a Plexiglass target we therefore get a fractional energy transfer of about 3%.

We now compare these experimental values for the fractional energy transfer to the shock-compressed region with the theoretical Eq. (9) derived in Section III c. Substitution of the averaged compression ratio $\varrho_1/\varrho_0 = 4.2$, the experimental Mach number $M = 1.2$ and the densities $\varrho_0 = 8.9 \times 10^{-2}$ g/cm³ and $\varrho_c = 1.67 \times 10^{-3}$ g/cm³ we obtain a theoretical value of $\eta_{ab} = 8.1 \times 10^{-2}$ for the fractional energy transfer in a solid hydrogen target. With the similar data for Plexiglass, $\varrho_1/\varrho_0 = 2.9$, $M = 2.0$, $\varrho_0 = 1.18$ g/cm³ and $\varrho_c = 3.03 \times 10^{-3}$ g/cm³ we obtain the value $\eta_{ab} = 3.8 \times 10^{-2}$.

The fractional energy transfer η_{ab}

	Theoretical	Experimental	from
Solid hydrogen	8.1%	8%	the kinetic energy
Plexiglass	3.8%	3%	blast wave model

Thus, the estimated experimental values are in good agreement with our theoretical approach. The difference in the two materials is basically due to the difference in the ratio ϱ_c/ϱ_0.

The initial stage of shock wave propagation in Plexiglass may be described by a constant time rate of work per unit surface for driving the shock wave. During the first few ns of the irradiation the shock wave in Plexiglass is approximately plane as can be observed from the framing picture in Fig. 6, and the shock wave trajectory in Fig. 17 may be given by a straight line.

The time rate of work is given by

$$\dot{W} = p_1 v_p = \varrho_0 v_s v_p^2$$

where $p_1 = \varrho_0 v_s v_p$ obtained from Eqs. (1) and (2) has been used. With the relation (11) this can be written as

$$\dot{W} = \varrho_0 u_s \left(\frac{u_s - a}{b}\right)^2$$

Substituting of ϱ_0 and the averaged shock velocity of 2.1×10^6 cm/s for the first 4 ns, we obtain

$$\dot{W} \cong 5 \times 10^{11} \text{ W/cm}^2 .$$

This energy flux into the shock-compressed region is obtained, as we have seen, with an efficiency of about 4%. Therefore, an effective laser intensity of $\dot{W}/\eta_{ab} \cong 1.3 \times 10^{13}$ W/cm² could be defined. This result is in agreement with the one-dimensional computer simulation presented in Fig. 10 and supports

the finding of the discussed two-dimensional effects of Section IVc.

Finally, it may be of interest to estimate the energy deposited in the interior of the target as a result of internal breakdown. A single breakdown, as observed in Fig. 7, may be considered as a point explosion and its energy is therefore estimated with the blast wave approximation described before. With the shock wave trajectory obtained from Fig. 7 b and an averaged value for $\alpha(\gamma)$ of $\cong 3$ in Eq. (10) a value for the deposited energy $E_0 \cong .2$ J is obtained. This energy is deposited inside the target before the absorbing plasma in front of the target is created. Thus, when focusing inside the target, a non-negligible part of the laser energy may be deposited in its interior, thus leading to a disturbance of the shock wave propagation.

V. Conclusions

Though thoroughly anticipated and discussed in the literature, laser-driven shock waves have not been directly observed and studied in the laboratory so far. The methods of framing and streak microphotography developed during the course of this experiment have now shown that laser-driven shock waves can be observed in transparent solids and investigated in a quantitative manner. The observations give direct access to what is often considered the most interesting quantity in laser-target interaction, namely the pressure echieved on irradiation of a solid target with a laser beam.

As a matter of fact, pressures in the Megabar range have been measured in light materials with a moderate laser intensity. The measured pressures could be verified in terms of known properties of the laser-heated, low-density plasma which acts as a driver for the shock wave. This comparison basically confirms the present understanding of laser-target interaction. A particularly interesting quantity, the efficiency of energy transfer to a laser-driven shock wave, was determined and found to agree with theoretical estimates.

It is clear, on the other hand, that the described experiment represents only a very first step to the useful application of laser-driven shock waves and is at present seriously limited by the low energy available from the laser. The need to concentrate the beam on a small area leads to a two-dimensional hydrodynamic flow which, as comparison with numerical simulations has shown, reduces the obtainable pressures considerably compared with those expected under a strictly one-dimensional flow. Also for the same reason, the accuracy in the evaluation of the experimental data is limited owing to the approximations which have to be made for lack of an exact description of the complicated experimental flow. Therefore, though the set of measured data seems consistent and basically understood, we cannot deal at the moment with questions of a quantitative nature such as possible modifications of the classical picture of plasma production by processes such as collision-free light absorption, flux limitation of electron heat conduction and fast ion blow-off [43]. Though obviously these processes have no dominant influence on the pressure measured in this experiment, their role cannot be assessed at the present stage with the desirable accuracy.

Preferably, these limitations should be overcome by the use of more powerful lasers now under construction. With the generation of plane shock waves which should then eventually be possible, the experimental results could be much more easily compared with theory and thus laser-generated shock waves could become a quantitative tool of high-pressure physics.

Acknowledgements

The author would like to thank Dr. R. Sigel for his encouragement and advice while this work was carried out. The many helpful discussions with Drs. K. Eidmann and P. Mulser are gratefully acknowledged. The author is indebted to Dr. S. Witkowski for his continued interest in the progress of this work. In addition the author would like to thank P. Sachsenmaier, E. Wanka, Mrs. H. Brändlein and G. Wirtz for their skillful help in the experimental work. This work was performed as part of the joint research programme of the Institut für Plasmaphysik and Euratom.

[1] P. J. McClung and R. W. Hellwarth, J. Appl. Phys. **33**, 828 [1962].
[2] N. G. Basov and O. N. Krokhin, Sov. Phys. JETP **19**, 123 [1964].
[3] J. M. Dawson, Phys. Fluids **7**, 981 [1964].
[4] J. Nuckolls, L. Wood, and G. Zimmerman, Nature **239**, 139 [1972]. — J. S. Clarke, H. N. Fisher, and R. J. Mason, Phys. Rev. Lett. **30**, 89 [1973]. — K. A. Brueckner, IEEE Trans. Plasma Sci. **1**, 13 [1973].
[5] S. I. Anisimov, JETP Lett. **16**, 404 [1972].

[6] E. Teller in "Laser Interaction and Related Plasma Phenomena", Vol. 3, Eds. H. J. Schwarz and H. Hora, Plenum Press, New York 1974, p. 3.

[7] J. W. Rae and A. Hertzberg, "On the possibility of simulating meteoroid impact by the use of lasers", CAL Rep. AI-1821-A-1, April 1964.

[8] J. F. Ready, "Effects of High-Power Laser Radiation", Academic Press, New York 1971.

[9] G. Charatis et al. in "Plasma Physics and Controlled Nuclear Fusion", Intern. Atomic Energy Agency, Vienna 1974, Paper IAEA-CN-33/F-1.

[10] R. Sigel, Z. Naturforsch. **25 a**, 488 [1970].

[11] C. G. Hoffmann, J. Appl. Phys. **45**, 2125 [1974].

[12] N. G. Basov, V. A. Boiko, V. A. Gribkov, S. M. Zakharov, O. N. Krokhin, and G. V. Sklizkov, Sov. Phys. JETP **34**, 81 [1972].

[13] M. H. Key, D. A. Preston, and T. P. Donaldson, in Proc. of the Seventh International Quantum Electronic Conference, Kyoto, Japan, 7—10 September 1970 (unpublished).

[14] C. G. M. van Kessel and R. Sigel, Phys. Rev. Lett. **33**, 1020 [1974].

[15] C. G. M. van Kessel, P. Sachsenmaier, and R. Sigel, "Proc. of the 11th Congress on High Speed Photography", London 1974, p. 437.

[16] K. Eidmann and R. Sigel, in "Laser Interaction and Related Plasma Phenomena", Vol. 3, Eds. H. J. Schwarz and H. Hora, Plenum Press, New York 1974, p. 667.

[17] P. Mulser, R. Sigel, and S. Witkowski, Phys. Lett. C (Physics Reports) **3**, 187 [1973].

[18] S. A. Akhmanov, R. V. Khohlov, and A. P. Sukhorukov, in "Laser Handbook", Vol. 2, Eds. F. T. Arecchi and E. O. Schulz-Dubois, North-Holland Publishing Company, Amsterdam 1972, p. 1151.

[19] A. Caruso and R. Gratton, Plasma Phys. **11**, 839 [1969].

[20] H. Puell, Z. Naturforsch. **25 a**, 1807 [1970].

[21] E. Cojocaru and P. Mulser, Plasma Physics **17**, 393 [1975].

[22] See References 17 and 25.

[23] E. J. Valeo and W. L. Kruer, Phys. Rev. Lett. **33**, 750 [1974].

[24] A. A. Galeev and A. Z. Sagdeev, Nuclear Fusion **13**, 603 [1973].

[25] Ya. B. Zel'dovich and Yu. P. Raizer, Physics of Shock Waves and High-Temperature Hydrodynamic Phenomena. English trans. (W. D. Hayes and R. F. Probstein, eds.), Academic Press, New York 1967.

[26] M. van Thiel, A. S. Kusubov, A. C. Mitchell, and V. W. Davies, Lawrence Livermore Laboratory Report No. UCRL-50108, 1966 (unpublished).

[27] M. van Thiel and B. J. Alder, Mol. Phys. **10**, 427 [1966].

[28] G. I. Kerley, LASL Reports No. LA-4760, 1971 and No. LA-4776, 1972 (unpublished).

[29] S. B. Kormer, Sov. Phys. Uspekhi **11**, 229 [1968].

[30] K. Eidmann and R. Sigel, in Proc. of the sixth European Conference on Controlled Fusion and Plasma Physics, Moscow 1973 (U.S.S.R. Academy of Sciences, Moscow 1973), p. 435.

[31] H. Salzmann, J. Appl. Phys. **44**, 113 [1973].

[32] L. I. Sedov, Similarity and Dimensional Methods in Mechanics, Gostekhizdat, 4th Edition 1957, English trans. M. Holt, ed.), Academic Press, New York 1967.

[33] G. I. Taylor, Proc. Roy. Soc. London **A 201**, 159 [1950].

[34] W. J. Rae, Rept. AI-1821-A-2, March 1965, Cornell Aeronautical Lab., Buffalo, New York.

[35] W. J. Rae and H. P. Kirchner, Proc. of the sixth Symp. on Hypervelocity Impact, Vol. II, Pt. I, August 1963, Firestone Tire and Rubber Co. ,p. 163.

[36] A. A. Birsh, M. S. Tarasov, and V. A. Tsakerman, Sov. Phys. JETP **11**, 15 [1960].

[37] M. H. Key and K. Eidmann, to be published.

[38] M. H. Key, K. Eidmann, C. Dorn, and R. Sigel, Phys. Lett. **48 a**, 121 [1974].

[39] F. Floux, J. F. Benard, D. Cognard, and A. Saleres, in "Laser Interaction and Related Plasma Phenomena", Vol. 2, Eds. H. J. Schwarz and H. Hora, New York 1972, p. 409, Plenum Press.

[40] H. C. Pant, private communication.

[41] D. Kohler, D. Giovanielli, R. P. Godwin, G. H. McCall, and M. M. Mueller, A. P. S. Plasma Phys. Meeting, October 28—31, 1974, Albuquerque, New Mexico.

[42] S. Ariga and R. Sigel, Int. Rep. IPP IV/81, Garching 1975.

[43] R. L. Morse and C. W. Nielson, Phys. Fluids **16**, 909 [1973]; R. E. Kidder and J. W. Zink, Nuclear Fusion **12**, 325 [1972].